AGU PUBLICATIONS

JGR

Journal of Geophysical Research: Atmospheres

RESEARCH ARTICLE

10.1002/2015JD023085

Key Points:
- Models do not simulate periods with out-of-phase winter and summer precipitation
- Observed out-of-phase winter and summer precipitation is anomalous
- Only the reconstructions consistently exhibits persistent dual-season drought

Correspondence to:
S. Coats,
sjc2164@columbia.edu

Citation:
Coats, S., J. E. Smerdon, R. Seager, D. Griffin, and B. I. Cook (2015), Winter-to-summer precipitation phasing in southwestern North America: A multicentury perspective from paleoclimatic model-data comparisons, *J. Geophys. Res. Atmos.*, *120*, 8052–8064, doi:10.1002/2015JD023085.

Received 7 JAN 2015
Accepted 7 JUL 2015
Accepted article online 14 JUL 2015
Published online 19 AUG 2015

Winter-to-summer precipitation phasing in southwestern North America: A multicentury perspective from paleoclimatic model-data comparisons

Sloan Coats[1,2], Jason E. Smerdon[1], Richard Seager[1], Daniel Griffin[3,4], and Benjamin I. Cook[1,5]

[1]Lamont-Doherty Earth Observatory, Columbia University, Palisades, New York, USA, [2]Department of Earth and Environmental Science, Columbia University, New York, New York, USA, [3]Department of Geography, Environment and Society, University of Minnesota, Minneapolis, Minnesota, USA, [4]Woods Hole Oceanographic Institution, Woods Hole, Massachusetts, USA, [5]NASA Goddard Institute for Space Studies, New York, New York, USA

Abstract The phasing of winter-to-summer precipitation anomalies in the North American monsoon (NAM) region 2 (113.25°W–107.75°W, 30°N–35.25°N—NAM2) of southwestern North America is analyzed in fully coupled simulations of the Last Millennium and compared to tree ring reconstructed winter and summer precipitation variability. The models simulate periods with in-phase seasonal precipitation anomalies, but the strength of this relationship is variable on multidecadal time scales, behavior that is also exhibited by the reconstructions. The models, however, are unable to simulate periods with consistently out-of-phase winter-to-summer precipitation anomalies as observed in the latter part of the instrumental interval. The periods with predominantly in-phase winter-to-summer precipitation anomalies in the models are significant against randomness, and while this result is suggestive of a potential for dual-season drought on interannual and longer time scales, models do not consistently exhibit the persistent dual-season drought seen in the dendroclimatic reconstructions. These collective findings indicate that model-derived drought risk assessments may underestimate the potential for dual-season drought in 21st century projections of hydroclimate in the American Southwest and parts of Mexico.

1. Introduction

The monsoon region of southwestern North America (Northern Mexico, Arizona, and New Mexico—hereinafter the Southwest) is characterized by a dual-season precipitation signal: winter precipitation occurs within transient midlatitude eddies, while summer precipitation is controlled by the North American monsoon (NAM) system. The NAM provides critical moisture relief after winter droughts, and given the considerable winter drought persistence in the region [e.g., *Stine*, 1994; *Herweijer et al.*, 2007; *Cook et al.*, 2007], precipitation deficits occurring in both the winter and summer seasons, i.e., dual-season drought, have the potential to greatly impact the Southwest. The phasing of winter and summer precipitation variability in the region, and the specific role played by the NAM in that phasing, is therefore important to understand and characterize.

The instrumental interval is marked by a relatively high occurrence of out-of-phase winter-to-summer precipitation anomalies in the Southwest [*Griffin et al.*, 2013], and there is dendroclimatic evidence that antiphasing of precipitation extremes may be a consistent feature of the Last Millennium [*Stahle et al.*, 2009]. Related research has focused on the dynamics that may drive such out-of-phase winter-to-summer precipitation anomalies. Along these lines, *Notaro and Zarrin* [2011] used a regional model to demonstrate that deep Rocky Mountain snowpack tends to hinder the poleward advance of the summer monsoon, and associated rainfall, into the Southwest (for the relationship between antecedent winter moisture and the summer monsoon, see also *Gutzler* [2000], *Higgins and Shi* [2000], and *Zhu et al.* [2005]). Additionally, *Castro et al.* [2001] found that tropical and extratropical Pacific sea surface temperatures (SSTs) influence the timing of the weakening of the Pacific jet and strengthening of the monsoon ridge, with a warm tropical Pacific delaying the monsoon onset and driving anomalously low summer precipitation. *Seager et al.* [2009], on the other hand, used multiple regression on observational and model data to demonstrate that a warm tropical Pacific produces increased precipitation in the northern NAM region during both winter and summer, with out-of-phase seasonal precipitation anomalies instead resulting from the canonical winter-to-summer shift from El Niño- to La Niña-like conditions [e.g., *Rasmusson and Carpenter*, 1982]. Importantly,

any out-of-phase seasonal precipitation relationship in the Southwest has considerable time instability even within the instrumental interval [*Gutzler*, 2000; *Zhu et al*., 2005]. Furthermore, a recent reconstruction of NAM variability using tree ring records of latewood width has established that the latter half of the 20th century exhibits potentially anomalous NAM behavior with regard to the prevalence of out-of-phase seasonal precipitation anomalies [*Griffin et al*., 2013]. The 20th century therefore may not be a characteristic period for defining the NAM precipitation climatology, its relationship to the winter climate regime, and the potential connections to the coupled atmosphere-ocean system.

Our investigation herein builds off the analyses of *Griffin et al.* [2013] using coupled model simulations to further assess assumptions about the stationarity of seasonal precipitation phasing relationships in the Southwest. We specifically apply the growing paradigm of paleoclimate model-data comparisons [e.g., *Anchukaitis et al*., 2012; *Ault et al*., 2013, 2014; *Coats et al*., 2013a, 2015a, 2015b; *Fernández-Donado et al*., 2012; *Phipps et al*., 2013; *Schmidt et al*., 2013] to characterize winter-to-summer precipitation phasing in the Southwest. We use independent tree ring-based reconstructions of NAM and winter precipitation variability [*Griffin et al*., 2013] in the NAM2 region (113.25°W–107.75°W, 30°N–35.25°N [*Gochis et al*., 2009]) for the period 1539–2008 Common Era (C.E.) as the basis for comparisons to the NAM dynamics in forced transient simulations of the Last Millennium (850–1850 C.E.) and the historical interval (1850–2005 C.E.), and in associated 500 year control simulations from the same models—all from the Coupled and Paleo Model Intercomparison Projects Phases 5 and 3 (CMIP5/PMIP3) [*Taylor et al*., 2012; *Schmidt et al*., 2011]. Four fundamental questions are addressed. (1) Are the teleconnections between the reconstructions and the tropical Pacific over the instrumental interval consistent with the lack of systematic in- or out-of-phase seasonal precipitation (section 3.1)? (2) Is there a seasonal precipitation phasing relationship, of either sign, in the models over the whole record or for shorter periods (e.g., the period with predominantly out-of-phase seasonal precipitation anomalies in the latter part of the instrumental record—section 3.3, Part 1)? (3) Are the model teleconnections in agreement with the reconstructions and observations, and are these consistent with the simulated seasonal precipitation phasing relationships (section 3.3, Parts 2 and 3)? And (4) Do models produce periods with predominantly in-phase winter-to-summer precipitation anomalies that lead to dual-season drought on interannual or decadal time scales (section 3.4)? The answers to these questions will clarify our understanding of seasonal precipitation phasing in the Southwest, while potentially elucidating the dynamics responsible for the real world and simulated phasing behavior. Furthermore, the assessment of reconstructed and simulated dual-season drought occurrence will help determine if state-of-the-art models are able to constrain the full character of risk associated with future hydroclimate change in the region.

2. Data

Reconstructed Standardized Precipitation Index (SPI) [*Mckee et al*., 1993] data are derived from a collection of more than 50 tree ring chronologies with seasonal resolution, the full details of which can be found in *Griffin et al.* [2013]. The data are reconstructed as a single time series for the NAM2 region using a forward stepwise multiple linear regression independently for both the winter (cool—October to April) and summer (warm—June to August) seasons over the period 1539 to 2008 C.E. This involves separating the systematic dependence of latewood (the dark, dense component of tree rings with a greater warm season signal) variability from the earlywood (light, less dense component with a greater cool season signal) variability using linear regression, with the effect of this adjustment being an increase in the summer precipitation signal [*Griffin et al*., 2011]. In the case of these reconstructions, the relationships between the instrumental and reconstructed variables are highly significant, positive, and stable [*Griffin et al*., 2013]. For comparison of these hydroclimate reconstructions to the observed sea surface temperature record we employ the Kaplan extended SST v2 product, which is a 5° latitude × 5° longitude gridded SST field for the period 1856 to present [*Kaplan et al*., 1998]. This is a well-validated SST data set that has been used for other paleoclimate model-data comparisons [*Coats et al*., 2013a, 2015a, 2015b].

All model output is from the CMIP5/PMIP3 archive (Table 1). We limit our analyses to the six models that produced and distributed simulations of the Last Millennium (LM) as part of the PMIP3 effort (at the time of our writing). These simulations span the period of 850–1850 C.E. and are forced with reconstructed time-varying exogenous forcings [*Schmidt et al*., 2011]. They have been appended to CMIP5 historical runs that span the period of 1850–2005 C.E. to produce a model record from 850 to 2005 C.E. Although these

Table 1. Model Information for the Analyzed CMIP5 Simulations

Modeling Center	Institute ID	Model Name
Beijing Climate Center, China Meteorological Administration	BCC	BCC-CSM1.1
National Center for Atmospheric Research	NCAR	CCSM4
NASA Goddard Institute for Space Studies	NASA GISS	GISS-E2-R
Institute Pierre-Simon Laplace	IPSL	IPSL-CM5A-LR
Japan Agency for Marine-Earth Science and Technology, Atmosphere and Ocean Research Institute (The University of Tokyo), and National Institute for Environmental Studies	MIROC	MIROC-ESM
Max-Planck-Intitut für Meteorologie (Max Planck Institute for Meteorology)	MPI-M	MPI-ESM-LR, MPI-ESM-P

simulations are not continuous, both the historical and LM simulations have the same model configuration and resolution. Consequently, if the simulations (particularly the historical run) have no drift, the discontinuity at 1850 should fall within the range of simulated climate variability. A large temperature drift in the Model for Interdisciplinary Research on Climate (MIROC) LM simulation [*Sueyoshi et al.*, 2013] violates this assumption, while a drift in the early centuries of the Goddard Institute for Space Studies (GISS) LM simulation [*Bothe et al.*, 2013] is likely to have less of an impact. While model drift undoubtedly impacts the hydroclimate variables assessed in this study, the effects are presumed to be moderate given the absence of drift in precipitation [*Sen Gupta et al.*, 2013]. The 500 year control simulations with constant preindustrial forcings (also from CMIP5) were additionally analyzed to aid in the interpretation of the LM model results. All model output has been regridded to a common 2.5° × 2.5° latitude-longitude grid to allow for direct comparison (this represents a coarsening of the model resolution for four out of six models).

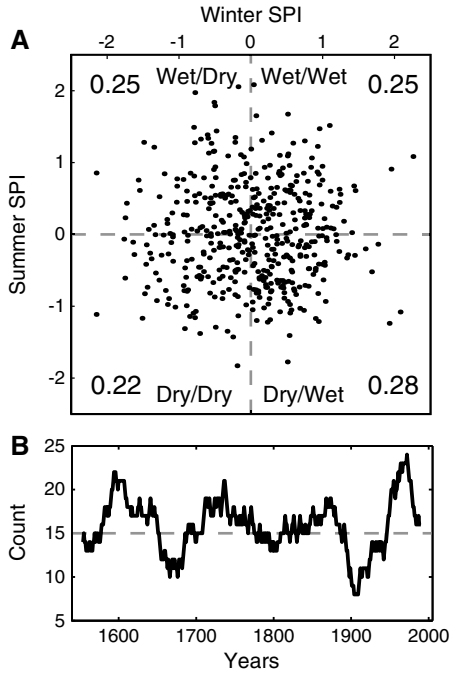

Figure 1. (a) Scatterplots of reconstructed SPI [*Griffin et al.*, 2013] for the winter (cool—October to April) and summer (warm—June to August) seasons over the period of 1539–2005 C.E., with the fraction of values in each quadrant listed within each quadrant box. (b) The time history of the winter-to-summer precipitation phasing. The black line represents a centered 30 year running count of opposing-sign winter and summer SPI anomalies. The dashed line is the threshold that indicates a neutral relationship between winter and summer precipitation anomalies.

For each model simulation, precipitation totals were converted to SPI for October–April (winter or cool season) and June–August (summer or warm season), with the α and β parameters of the gamma distribution computed for the 1896–2005 period. These choices match the SPI-reconstructed target variable in the above discussed dendroclimatic reconstructions. For each model a hydroclimate time series was calculated by spatially averaging the SPI over the NAM2 region.

3. Results and Discussion

3.1. Reconstruction Dynamics and Phasing

Griffin et al. [2013] note that the number of years with in- and out-of-phase seasonal precipitation anomalies is approximately equal over the length of their reconstructions, and, on that basis, they declare that there is no systematic seasonal precipitation phasing relationship in the NAM2 region. This is shown in Figure 1a, indicating an approximately equal probability of any reconstructed year having a wet winter and summer, dry winter and summer, or opposite-signed precipitation anomalies in the two seasons. Nevertheless, to assess the possibility that shorter periods may exhibit predominantly in- or out-of-phase seasonal precipitation anomalies, the number of out-of-phase years was calculated for a sliding 30 year window in the reconstructions and plotted in Figure 1b (following *Griffin et al.* [2013]—hereinafter the count value). Despite the lack of a systematic seasonal precipitation phasing relationship, the reconstructed SPI record is punctuated by shorter periods when out-of-phase events congregate (most notably in

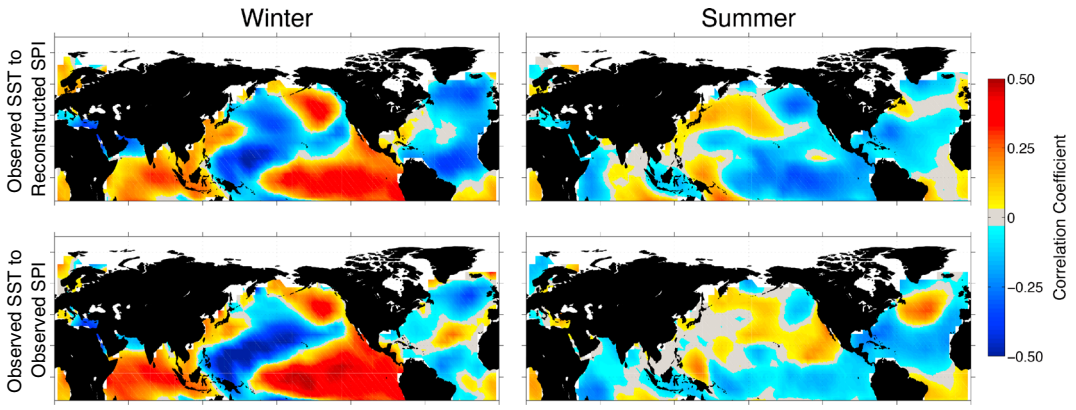

Figure 2. Maps of Pearson's correlation coefficients calculated between (left) winter (DJF) or (right) summer (JJA) SPI and SSTs. All results are shown for 1950–2005 C.E., the overlapping period of the reconstructions, the observed SST data set [*Kaplan et al.*, 1998] and the period of good coverage over the NAM2 region for the observed precipitation data set (GPCC [*Becker et al.*, 2013]). The plotted domain is 180°W–180°E, 40°S–90°N.

the mid-to-late 20th century), as well as periods with predominantly in-phase seasonal precipitation anomalies (the beginning of the 20th century). In both cases these are significant against the null hypothesis that the phasing could occur randomly (not shown), which suggests that there are atmosphere-ocean dynamical associations underlying the most in- and out-of-phase periods in the reconstructions. There are a number of dynamics that have been implicated as having the potential to drive seasonal precipitation phasing. For out-of-phase winter-to-summer precipitation anomalies these include (1) opposite-sign winter and summer teleconnections tied to same-sign winter and summer SST anomalies [e.g., *Castro et al.*, 2001], (2) a winter-to-summer shift in tropical Pacific SSTs and a same-sign winter and summer teleconnection [e.g., *Seager et al.*, 2009], and (3) the land surface feedback described in the Introduction [e.g., *Notaro and Zarrin*, 2011]. To determine which, if any, of these dynamics are consistent with the SPI reconstructions of *Griffin et al.* [2013], the relationship between the tropical Pacific and hydroclimate over the NAM2 region will be analyzed using an instrumental SST data set and the overlapping period in the SPI reconstructions (1856–2005 C.E.—hereinafter observation to reconstructions). We do not make an explicit attempt to analyze land surface feedbacks (point 3), but it is worth noting that land surface feedbacks are expected to be present in the observational and reconstructed data and are not separable from the observation to reconstructions teleconnection dynamics analyzed herein. Additionally, we do not analyze potential drivers of seasonal precipitation phasing that receive less attention in the literature, for instance forcing from tropical or extratropical Atlantic SSTs [e.g., *Kushnir et al.*, 2010].

There is evidence that an evolution from El Niño- to La Niña-like conditions going from winter to summer is possible (e.g., in 1998 [see also *Seager et al.*, 2009]) but that tropical Pacific SST anomalies can also persist between seasons [e.g., *Rasmusson and Carpenter*, 1982]. The seasonal evolution of tropical Pacific SST anomalies, along with the winter and summer teleconnections, will determine the impact of the tropical Pacific Ocean on seasonal precipitation phasing in the Southwest. To determine which seasonal evolution is more probable, we assess the winter versus following summer SST anomalies over the Niño3.4 region (170°W–120°W, 5°S–5°N). There is a slight positive relationship between winter and summer tropical Pacific SST anomalies (not shown), indicating a tendency for same-sign SST anomalies to persist from winter to summer. Nevertheless, this relationship is weak but significant at the 95% level, with a squared Pearson's correlation coefficient (R^2) of 0.13.

Figure 2 characterizes the winter and summer teleconnections between SPI in the NAM2 region and the winter (December-January-February (DJF)) and summer (June-July-August (JJA)) SST fields for the 56 years (1950–2005 C.E.) that are common to the observed SST data set [*Kaplan et al.*, 1998], the reconstructions, and the period of good coverage over the NAM2 region in an observed precipitation data set from the Global Precipitation Climatology Center (GPCC) [*Becker et al.*, 2013, herinafter observed]. The observation to reconstructions and observed teleconnections are in good agreement throughout the tropical and extratropical Pacific, with the exception of an area of positive correlation off the coast of western North America in summer that is only present in the observations. Importantly, in both cases the teleconnection patterns are of opposite

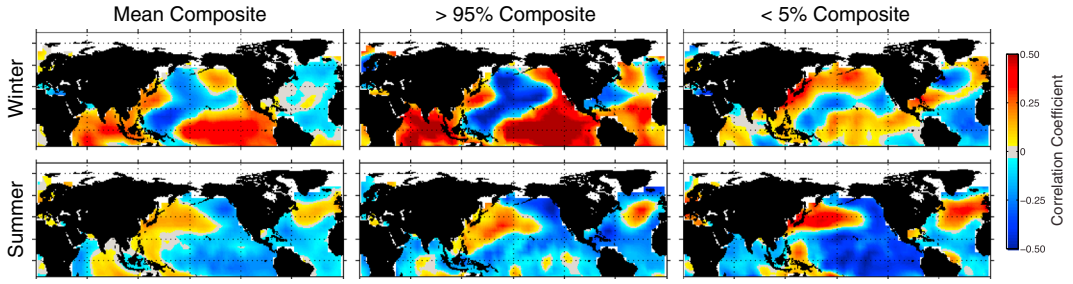

Figure 3. (left column) Mean composite contains the average maps of Pearson's correlation coefficients calculated between winter (DJF) or summer (JJA) reconstructed SPI and observed SSTs [*Kaplan et al.*, 1998] for random 30 year periods between 1856 and 2005 C.E. The (middle column) >95% composite and (right column) <5% composite columns contain the 30 year segments with the greater than 95th percentile or less than 5th percentile of average correlation coefficients over the Niño3.4 region (170°W–120°W, 5°S–5°N). The plotted domain is 180°W–180°E, 40°S–90°N.

sign in winter and summer and of similar magnitude. The teleconnection dynamics, however, are complicated by the fact that the strength and character of the observation to reconstructions summer teleconnection varies over the full period of overlap between the reconstructions and SST data set (1856–2005 C.E.—Figure 3).

Collectively, the seasonal evolution of tropical Pacific SSTs and the average teleconnections suggest a preference for out-of-phase seasonal precipitation (same-sign SST anomalies and opposite-sign teleconnections). Nevertheless, the summer teleconnection is potentially nonstationary (Figure 3), and the tropical Pacific exhibits only a weak tendency for same-sign SST anomalies to persist from winter to summer. Together, this makes a systematic out-of-phase seasonal precipitation relationship unlikely, which is consistent with the roughly equal probability of reconstructed seasonal precipitation anomalies being in or out of phase in any given year [*Griffin et al.*, 2013]. Nevertheless, any nonstationarity of the summer teleconnection has the potential to produce shorter periods where the seasonal precipitation phasing relationship is more or less out of phase (e.g., more out of phase when the summer teleconnection to the tropical Pacific is particularly strong and negative as in the <5% composite in Figure 3).

3.2. Do Models Have a NAM?

Before analyzing simulated seasonal precipitation phasing and the dynamics thereof, it is necessary to determine that the PMIP3 models simulate a NAM. To do so, the simulated precipitation climatologies and standard deviations over the NAM2 region are plotted in Figure 4. Only the Community Climate System Model (CCSM), MIROC, and Max-Planck-Institut (MPI) models simulate a realistic May–June climatological dry period followed by a substantial monsoon onset. The MPI and CCSM models have a particularly robust July-August-September precipitation peak with monsoon retreat by October. MIROC has a summer precipitation peak, but the September maximum and wet October are not realistic. In contrast, Beijing Climate Center (BCC), Institute Pierre-Simon Laplace (IPSL), and GISS all lack any summer precipitation maximum. All of the model standard deviations are inflated relative to the observations.

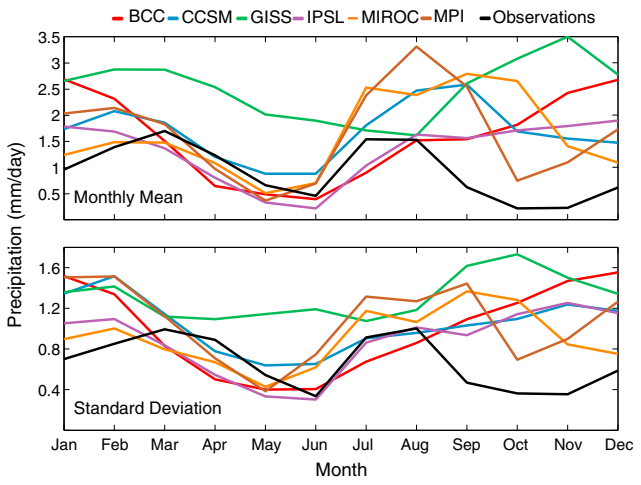

Figure 4. (top) The average monthly precipitation in the NAM2 region for the full LM simulations and observational data from the Global Precipitation Climatology Center (1901–2010 [*Rudolf et al.*, 1994]). (bottom) The interannual standard deviation of monthly precipitation for all of the models and the observations.

For the purposes of analyzing winter-to-summer precipitation phasing relationships, only the CCSM and MPI simulations will be retained. While the MIROC model appears to have a NAM, the precipitation

climatology is not as realistic as the CCSM and MPI models and the LM simulation has the aforementioned significant drift [*Sueyoshi et al.*, 2013]. CCSM and MPI are also the same models (of the LM simulation subset of CMIP5/PMIP3) that were determined to have a sufficiently realistic NAM for the projections of Southwest monsoon rainfall in *Cook and Seager* [2013]. Moreover, *Langford et al.* [2014] provide a detailed analysis of the NAM dynamics in all of the CMIP5 models and find a positive relationship between model resolution and the realism of NAM dynamics; CCSM and MPI are the two highest-resolution simulations of the Last Millennium.

3.3. Seasonal Precipitation Phasing and the Model Dynamics

Here we analyze the seasonal precipitation phasing in the models (Part 1) and assess the consistency of this phasing with regard to the potential atmosphere-ocean dynamical influences on seasonal precipitation phasing outlined in section 3.1 and the model specific dynamical characteristics (Parts 2 and 3). The limited model output prevents a full analysis of the presence of land surface feedbacks (point 3 in section 3.1); however, the potential biases in simulated snow physics [e.g., *Foster et al.*, 1996], coarse model resolution preventing a realistic simulation of orographic features, and the nondynamic land surface and vegetation models in CCSM and MPI make a realistic role for simulated land surface feedbacks unlikely.

3.3.1. Seasonal Precipitation Phasing

Figure 5 presents scatterplots of winter- and summer-simulated SPI anomalies (1539–2005 C.E.) as a characterization of the winter-to-summer precipitation phasing relationships (Figure 5a). These indicate that similar to the reconstructions [*Griffin et al.*, 2013], there is no systematic seasonal precipitation phasing relationship between winter and summer in the CCSM and MPI simulations (56% and 54% of years are in-phase, respectively).

Despite the fact that the models do not exhibit a systematic seasonal precipitation phasing relationship, the high occurrence of out-of-phase seasonal precipitation anomalies in the latter part of the instrumental record (e.g., Figure 1b) [*Griffin et al.*, 2013] suggests that shorter periods may exhibit predominantly in- or out-of-phase seasonal precipitation anomalies. In contrast to both the instrumental data and the reconstructions, the models do not simulate periods with seasonal precipitation anomalies that are predominantly out-of-phase. This is indicated by the fact that the number of out-of-phase years over the 30 year windows in Figure 5b rarely, and never by a large margin, exceeds 15—the threshold that indicates a neutral relationship between winter and summer precipitation anomalies. The models do, however, have multiple periods with predominantly in-phase winter and summer SPI anomalies (e.g., the 30 year period beginning in 1690 in CCSM and 1680 in MPI). It is additionally worth noting that this model behavior does not appear to be dependent on the forcing—control simulations from the same models reproduce approximately the same phasing characteristics (Figures 6c and 6d).

To test the significance of the in-phase periods in the models against the null hypothesis that this phasing can occur randomly, a 50,000 year autocorrelation- and distribution-preserving surrogate time series was created for both the winter and summer SPI anomalies from each data set. The number of years with out-of-phase anomalies for each 30 year period in the surrogate time series was counted, and the upper and lower 99th percentile of these values were chosen as the significance thresholds. These bounds were 21 and 9 in each model, indicating out-of-phase significance against the null hypothesis for 30 year count values above 21 and in-phase significance for 30 year count values below 9. Multiple count values fall below the lower bound of the significance thresholds, indicating that there are in-phase periods in both model simulations that would not be expected to occur by chance alone. Because these in-phase periods cannot be explained by random chance, there may instead be atmosphere-ocean dynamical associations in the models that underlie their origin.

3.3.2. Simulated Seasonal El Niño–Southern Oscillation Evolution

The impact of the tropical Pacific Ocean on seasonal precipitation phasing will depend on whether same-sign SST anomalies persist from winter to summer [e.g., *Rasmusson and Carpenter*, 1982]. Nevertheless, an evolution from El Niño- to La Niña-like conditions going from winter to summer is also possible, for instance, in 1998 [see also *Seager et al.*, 2009]. To assess the probability of same-sign SST anomalies occurring in winter and summer, Figure 6 shows a centered 30 year running count (with 30 years chosen to match the assessment of seasonal precipitation phasing in *Griffin et al.* [2013]) of same-sign winter-to-summer SST anomalies in the Niño3.4 region (170°W–120°W, 5°S–5°N). If the values in Figure 6 are at 15 (the dashed line), the probability of SST anomalies persisting and changing sign between winter and summer are equal (greater than 15

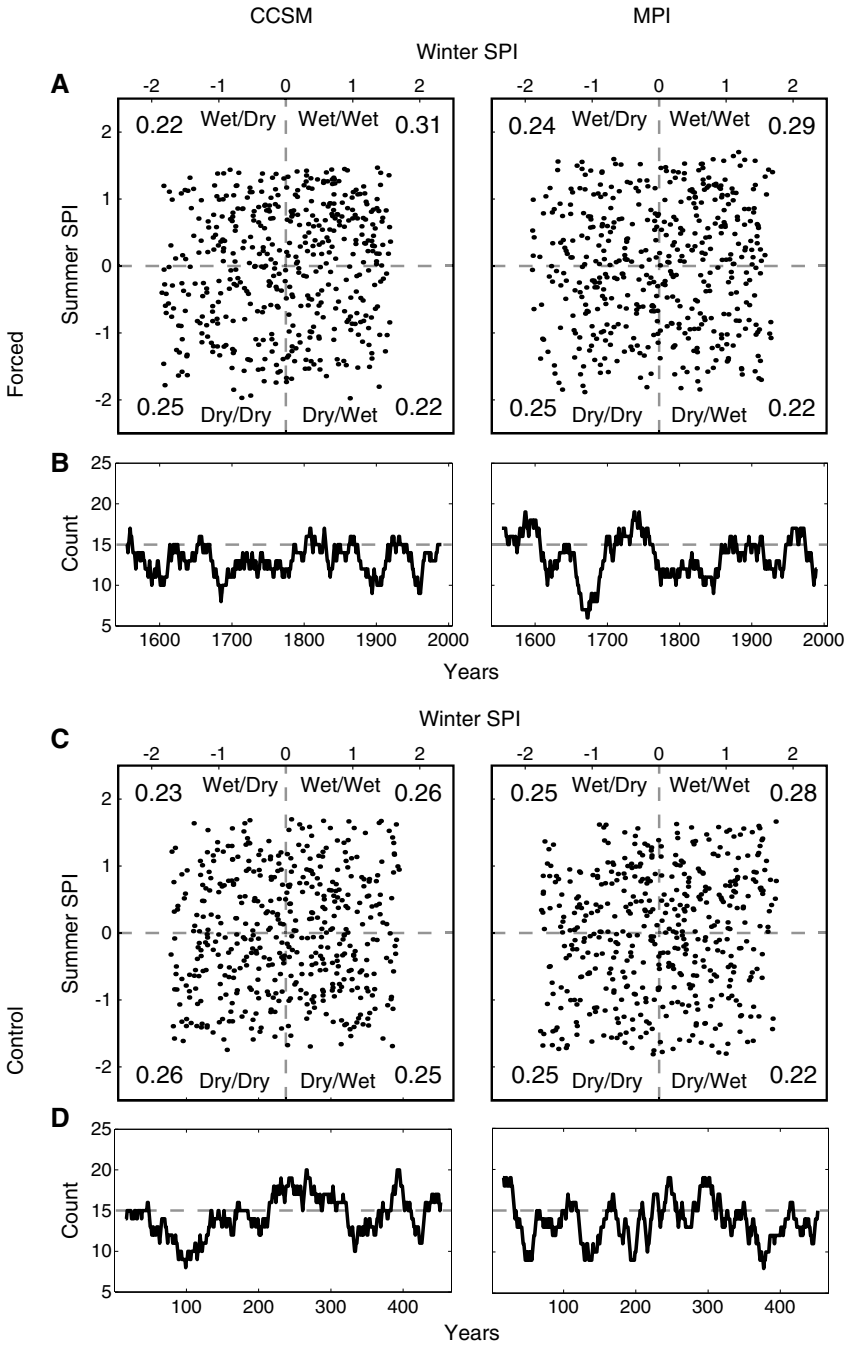

Figure 5. (a) Scatterplots of simulated SPI for the winter (cool—October to April) and summer (warm—June to August) seasons over the period of 1539–2005 C.E., with the fraction of values in each quadrant listed within each quadrant box. (b) The time history of the winter-to-summer precipitation phasing. The black line represents a centered 30 year running count of opposing-sign winter and summer SPI anomalies. The dashed line is the threshold that indicates a neutral relationship between winter and summer precipitation anomalies. (c and d) The same plots for 500 year control runs from the CCSM and MPI models.

indicates a preference for SST anomalies to persist between winter and summer). The CCSM model exhibits a weak preference for the persistence of tropical Pacific SST anomalies from winter to summer (count values just above 15—Figure 6). In contrast, the MPI model has consistently high count values in Figure 6, with a strongly positive Pearson's linear correlation coefficient between winter and summer tropical Pacific

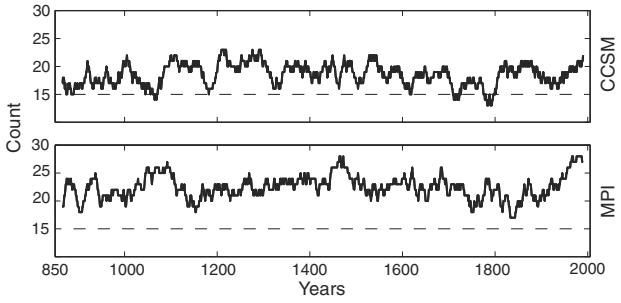

Figure 6. The time history of the winter-to-summer SST anomalies in the Niño3.4 region (170°W–120°W, 5°S–5°N). The black line represents a centered 30 year running count of same-sign winter and summer SST anomalies. The dashed line is the threshold that indicates a neutral relationship between winter and summer SST anomalies.

SSTs for the period of 1539–2005 C.E. (R^2 of 0.41). This suggests that the persistence of same-sign tropical Pacific SST anomalies from winter-to-summer will occur more frequently in MPI relative to CCSM (positive correlation and R^2 of 0.06) or the observations (R^2 of 0.13 in section 3.2). The discrepancy between the two models is potentially related to their representation of the El Niño–Southern Oscillation (ENSO). The CCSM model, for instance, has a stronger and more regular ENSO [*Coats et al.*, 2015a], although both models, and these specific simulations, have well-validated and realistic ENSO [e.g., *Coats et al.*, 2013b, 2015b]. In summary, both models exhibit tropical Pacific SST anomalies that tend to persist from winter to summer, although this behavior is stronger in MPI relative to both CCSM and the observations.

3.3.3. Simulated Teleconnections

In both models the winter teleconnection between the NAM2 region and the tropical Pacific is positive and characteristic of the observed teleconnection in sign, magnitude, and spatial features (Figure 7). The MPI model exhibits a moderately negative summer teleconnection between NAM2 SPI and the tropical Pacific that is again largely characteristic of the observation to reconstructions and observed summer teleconnections (Figure 7). In contrast to the observation to reconstructions and MPI dynamics, the CCSM model exhibits a weakly positive summer teleconnection (Figure 7). This is of the same sign as the winter teleconnection in the CCSM model, which exhibits winter precipitation variability that is tightly coupled to the tropical Pacific on both interannual and longer time scales [*Coats et al.*, 2015a, 2015b].

The longer model simulations allow for a more complete assessment of the stationarity of the dynamical relationships between NAM2 hydroclimate and the tropical Pacific Ocean. To do so, the LM runs were divided into 56 year segments to match the length of the National Centers for Environmental Prediction (NCEP)/National Center for Atmospheric Research (NCAR) reanalysis record [*Kalnay et al.*, 1996], generating a time-slice ensemble of 17 members for each LM run. The use of nonoverlapping 56 year segments maintains consistency with *Coats et al.* [2013b, 2015a, 2015b]. For each segment the correlation between the Niño3.4 index and the 200 mb geopotential height field (again following *Coats et al.* [2013b, 2015a, 2015b]) was calculated for both the winter (DJF) and summer (JJA) seasons and compared to the 56 year (1949–2005 C.E.) patterns from the reanalysis, using the centered pattern correlation statistic (CPCS) [*Santer et al.*, 1995]. The range in the CPCS is thus interpreted as a measure of the temporal stationarity of the teleconnection within a given model following *Coats et al.* [2013b] and is plotted in Figure 8. The analysis described above indicates

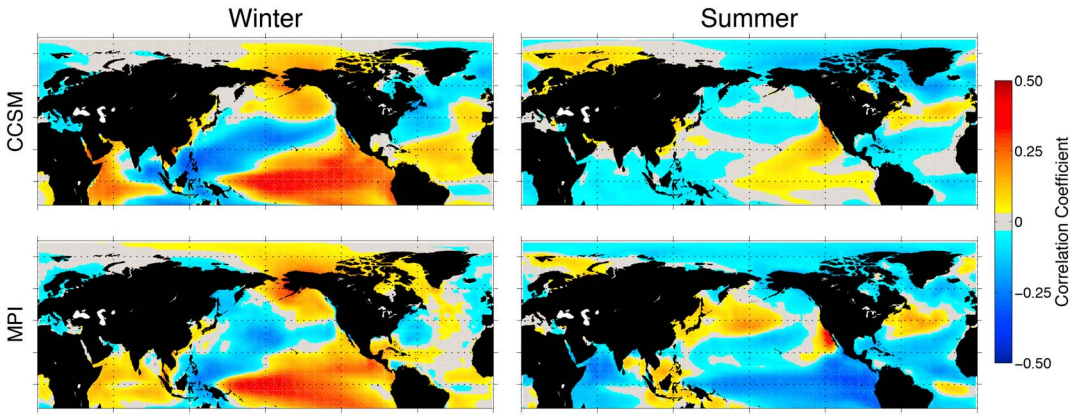

Figure 7. The same as Figure 2 but for the (top) CCSM and (bottom) MPI simulations (calculated over their full duration). The plotted domain is 180°W–180°E, 40°S–90°N.

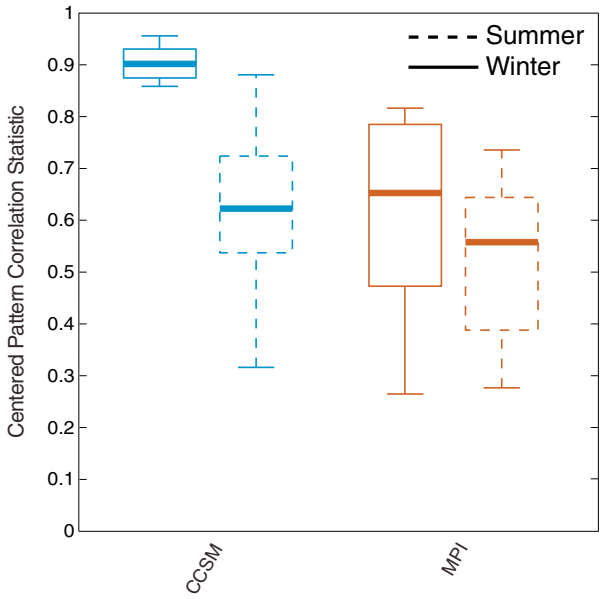

Figure 8. Winter (DJF) and summer (JJA) teleconnection (defined as the Niño3.4 index correlated with 200 mb geopotential height) stationarity, as measured by the centered pattern correlation statistic (CPCS) over North America (160°W–50°W, 20°N–70°N) between the teleconnection patterns estimated from the NCEP-NCAR reanalysis and nonoverlapping 56 year segments from the models. The box plots indicate the 75th and 25th percentiles of the CPCS statistic across the segments in the respective coupled model runs with the median as the bolded line and the whiskers showing the full data excluding outliers. Full methodology can be found in *Coats et al.* [2013b].

that the CCSM winter teleconnection is highly stationary, while the summer teleconnection is not. Neither the winter nor summer teleconnections are stationary through time in MPI, and more generally, Southwestern hydroclimate is less tightly coupled to the tropical Pacific in MPI relative to the CCSM model [*Coats et al.*, 2015a].

3.3.4. Dynamical Conclusions

We now summarize the dynamics for each model and how they relate to the lack of a systematic seasonal precipitation phasing relationship, while in the next two paragraphs we reconcile these dynamics with the shorter periods of significantly in-phase seasonal precipitation anomalies (Part 1). CCSM exhibits positive winter and summer teleconnections. These teleconnection characteristics suggest that in-phase seasonal precipitation anomalies are more likely to occur. The weak average magnitude and nonstationarity of the summer teleconnection in CCSM (Part 3), as well as the weak tendency for tropical Pacific SSTs to persist from winter to summer (Part 2), however, make seasonal precipitation phasing that is systematically in-phase unlikely. In MPI, the opposite-sign winter and summer teleconnections suggest that out-of-phase seasonal precipitation anomalies should occur with a higher probability. Such phasing is made less likely, however, due to the highly nonstationary teleconnections in MPI (Part 3) and generally weaker control of the tropical Pacific on North American hydroclimate in the model [*Coats et al.*, 2015a, 2015b].

The presence of shorter periods that are significantly in-phase in the MPI simulation (Part 1) is surprising given the winter and summer teleconnection characteristics outlined in Parts 2 and 3 of this section. The MPI model, nevertheless, has a high degree of nonstationarity in its teleconnections. The periods of predominantly in-phase seasonal precipitation anomalies in MPI may be indicative of the importance of this nonstationarity, with the tropical Pacific influence on the Southwest either weakening enough to allow other atmosphere-ocean dynamics to dominate the precipitation phasing relationship (e.g., tropical or extratropical Atlantic SSTs), or changing such that the tropical Pacific actually makes in-phase seasonal precipitation anomalies more likely than out-of-phase anomalies. Analysis of the 5% of 30 year periods in the MPI model with the most in-phase seasonal precipitation suggests a robust weakening of the summer teleconnection, consistent with this interpretation (not shown).

The periods of significantly in-phase seasonal precipitation in the CCSM model are consistent with the teleconnection and ENSO behavior outlined in Parts 2 and 3 of this section. Nevertheless, this phasing relationship might be expected to be stronger given a more stationary summer teleconnection or a greater frequency of same-sign tropical Pacific SST anomalies persisting from winter-to-summer simulated within CCSM.

3.4. Dual-Season Drought on Interannual and Decadal Time Scales in the NAM2

The periods with a significant number of in-phase winter-to-summer precipitation anomalies in the models and reconstructions are suggestive of a potential for frequent in-phase dry or dual-season drought years (defined as having winter and summer precipitation below the mean). This is only weakly true of the data analyzed herein, with in-phase dry years, or dual-season drought, occurring 28, 30, and 27% of the time (in CCSM, MPI, and the reconstructions, respectively) in the 30 year periods that fall above the 95th percentile

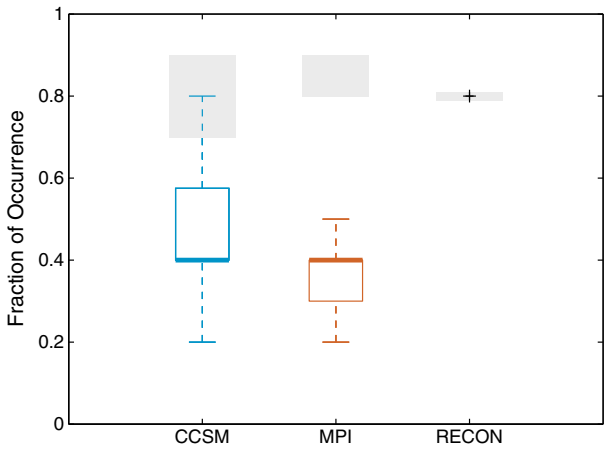

Figure 9. Fraction of the 10 largest winter and summer droughts (as identified using the 2S2E drought identification metric) that are contemporaneous in time for the full reconstructions and for a sliding 467 year (length of the reconstructions) window across the full 1156 year model record. The gray shaded region is the 99% confidence interval for these values as determined by an autocorrelation- and distribution-preserving bootstrapping method. The box plots indicate the 75th and 25th percentiles of the fraction of overlapping droughts across the segments in the respective coupled model runs with the median as the bold line and the whiskers showing the full data excluding outliers.

for number of years with in-phase seasonal precipitation anomalies. These values are 25, 25, and 22% when all 30 year periods are considered.

A distinction can be made between these interannual dual-season droughts and decadal-scale or persistent drought (e.g., the megadroughts in the paleoclimate record of the Southwest, which may or may not have been dual season in character [*Stine*, 1994; *Herweijer et al*., 2007; *Cook et al*., 2007]). Given the multidecadal variability in the phasing of precipitation it is unclear if the models or the reconstructions will exhibit decadal-scale dual-season drought in the NAM2 region. To test this, the model and reconstructed SPI time series were used to identify persistent droughts, with a drought commencing after two consecutive years of negative SPI and continuing until two consecutive years of positive SPI (hereinafter the two start, two end, or 2S2E drought definition—see *Coats et al*. [2013a] for further details). As in *Coats et al*. [2013a], the identified droughts were ordered using a drought density rank in which SPI values were summed from the first to the last year of each identified drought and then ranked based on the largest negative value of this sum. Figure 9 plots the percentage of times that the 10 highest-ranking winter and summer droughts overlap in time (defined by any number of overlapping drought years), with the droughts identified and ranked using the 2S2E drought definition and the ranking methodology described above; results are shown for the full reconstructions and for a sliding 467 year (length of the reconstructions) window across the full 1156 year model record (this produces a range in the contemporaneity of the 10 highest-ranking winter and summer droughts for each model, which are represented as box plots in Figure 9). To test the significance of these associations, 5000 pairs of independent surrogate time series with the same distribution and autocorrelation structure as the respective winter or summer SPI anomalies were produced for each data set. For the reconstructions, the contemporaneity between the 10 highest-ranking winter and summer droughts for each surrogate pair was calculated, with the 99% level of these values being considered significant. For the CCSM and MPI models, 5000 pairs of surrogate time series were produced for each 467 year window. For each of these windows, contemporaneity between the 10 highest-ranking summer droughts and the 10 highest-ranking winter droughts for each surrogate pair was again calculated, and the 99% level was recorded to produce a significance range (the gray shaded regions in Figure 9).

For the reconstructions, 80% of the 10 highest-ranking winter and summer droughts are coincident in time, a value that is equal to the 99% level of the surrogate indices. This is a remarkable result and suggests that over the last 500 years persistent drought in the NAM2 region has consistently been dual-season in character. It must be noted, however, that while the reconstruction methodology separates the winter and summer signals on interannual time scales [e.g., *Griffin et al*., 2013], the low-frequency winter and summer signals are more challenging to parse given the short instrumental record. It is thus difficult to determine unequivocally that persistent dual-season drought does not result from low-frequency memory within the proxy itself [e.g., *Bunde et al*., 2013]. Nevertheless, it is worth hypothesizing how persistent dual-season drought occurs given the teleconnections outlined in section 3.1. Dual-season drought will require reduced precipitation in both winter and summer. This will involve less precipitation delivery from the winter Pacific storm track along with a weaker or less northward extended NAM—a combination that the average observation to reconstructions teleconnection characteristics suggests is relatively unlikely. Nonstationarity in the teleconnection dynamics is a potential source of this discrepancy, and along these lines, persistent dual-season drought may occur in

periods when the teleconnection or tropical Pacific variability changes such that in-phase precipitation anomalies are more likely to occur. A second possibility is that winter drying is driven by a persistently cold tropical Pacific while summer drying is dominated by a persistently warm tropical Atlantic—as suggested in Figure 2 (see also *Kushnir et al.* [2010] and as suggested as the cause of the Medieval Climate Anomaly megadroughts by *Oglesby et al.* [2012] and *Feng et al*. [2008]). The negative correlation in summer between the reconstructions and the tropical Atlantic, however, appears weaker than the summer connection to the tropical Pacific (Figure 2), although some nonstationarity of this relationship is suggested in Figure 3. Additionally, there may be land surface or other feedbacks that become important during severe events or on long time scales. One potential example is the vegetation or dust aerosol feedback, both of which have been shown to be important in determining the spatial scale and magnitude of drought in the Great Plains region of the United States [e.g., *Cook et al*., 2013].

For the models, only the CCSM simulation has 467 year periods with a significant association between the 10 highest-ranking winter and summer droughts, although the majority of the 467 year periods fall well below the significance range (97% of the periods are not individually significant at the 99% level). This indicates that the models, for the most part, do not simulate the persistent dual-season drought exhibited by the reconstructions (*Bunde et al.* [2013] note a similar discrepancy between paleoclimate reconstructions and model simulations). Nevertheless, the greater frequency (relative to MPI) of persistent dual-season drought in the CCSM model is a likely function of the model's specific dynamical characteristics. While both the MPI and CCSM models have been shown to exhibit large-magnitude mean-state changes in the tropical Pacific, the CCSM model more consistently relates these changes to winter hydroclimate in the Southwest [*Coats et al.*, 2015a]. Furthermore, the weak but positive summer teleconnection in the CCSM model, as compared to the moderately negative summer teleconnection in MPI, increases the likelihood that winter and summer SPI anomalies will be of the same sign. It is difficult to assess this model behavior in the context of the shorter reconstruction interval, which may be anomalous in its connection between persistent winter and summer droughts (e.g., similar to a significant period in the CCSM model). The MPI model, however, appears to underestimate the risk of persistent dual-season drought, a characteristic that may or may not be shared by the CCSM model (Figure 9).

4. Conclusions

Multidecadal variability in the phasing of winter-to-summer precipitation anomalies in the Southwest is a robust characteristic of models and tree ring-based reconstructions of NAM and winter precipitation variability [*Griffin et al.*, 2013]. While the latter part of the instrumental interval is marked by relatively frequent out-of-phase winter-to-summer precipitation anomalies, models do not reproduce periods with winter-to-summer precipitation anomalies that are predominantly out-of-phase, and the reconstructions indicate that such behavior is anomalous over a 467 year interval. The CCSM and MPI models, instead, exhibit multiple periods of predominantly in-phase winter-to-summer precipitation anomalies. The model preference for periods with an in-phase seasonal precipitation relationship creates the possibility that dual-season drought will occur frequently in the simulations. Nevertheless, only the reconstructions and CCSM model (though inconsistently) exhibit significant periods of persistent or decadal-scale dual-season drought.

These results have potential implications for efforts to project the future hydroclimate of the Southwest and to provide seasonal forecasts of the summer monsoon. First, models do not appear to consistently exhibit periods of persistent dual-season drought that are comparable to those in the reconstructions. Whether or not this is realistic, such model behavior must be better understood because models may be underrepresenting the risk of future year-round drought in the Southwest. Second, nonstationarity of simulated teleconnections of the tropical Pacific to North America has been demonstrated [*Coats et al.*, 2013b]. In the MPI model in particular, nonstationarity appears to impact seasonal precipitation phasing in the Southwest, as the model exhibits no systematic seasonal precipitation phasing relationship despite ENSO dynamics and a tropical Pacific teleconnection that should produce out-of-phase seasonal precipitation anomalies. Understanding whether teleconnection nonstationarity is physically reasonable may elucidate whether nonstationarity is an important driver of the real-world seasonal precipitation phasing behavior. Finally, the out-of-phase character of winter-to-summer precipitation anomalies that has guided much of the dynamical research on the NAM over the past two decades appears highly nonstationary in the

real world [*Griffin et al.*, 2013] and completely absent in state-of-the-art fully coupled general circulation models. While it is possible that this results from biases inherent to the models or the reconstruction methodology, it is likely necessary to expand the paradigm through which we view seasonal precipitation phasing in southwestern North America. Along these lines, a more comprehensive exposition of the dynamics that drive the phasing relationship between winter and summer precipitation anomalies in the real world, as has been initiated herein, will allow for more robust seasonal forecasts of Southwestern hydroclimate and in particular of the NAM.

Acknowledgments

This work was supported by NOAA award NA11OAR4310166 and NSF award AGS-1243204. Additional support for B.I. Cook was provided by National Aeronautics and Space Administration Modeling Analysis and Prediction Program WBS 281945.02.04.02.74 ("Cool and Warm Season Moisture Reconstruction and Modeling over North America"). Additional support for D. Griffin was provided by the NOAA Climate and Global Change Postdoctoral Fellowship. We acknowledge the World Climate Research Programme's Working Group on Coupled Modelling, which is responsible for CMIP, and we thank the climate modeling groups (listed in Table 1) for producing and making available their model output. For CMIP the U.S. Department of Energy's Program for Climate Model Diagnosis and Intercomparison provides coordinating support and led development of software infrastructure in partnership with the Global Organization for Earth System Science Portal. The data for this paper are available from the Program for Climate Model Diagnosis and Intercomparison (http://cmip-pcmdi.llnl.gov/cmip5/). LDEO contribution 7917. We thank three anonymous reviewers for their comments that improved the quality of this manuscript. We, further, thank Haibo Liu and Naomi Henderson for their considerable computational support.

References

Anchukaitis, K. J., et al. (2012), Tree rings and volcanic cooling, *Nat. Geosci.*, *5*, 836–837, doi:10.1038/ngeo1645.

Ault, T. R., J. E. Cole, J. T. Overpeck, G. T. Pederson, S. St. George, B. Otto-Bliesner, C. A. Woodhouse, and C. Deser (2013), The continuum of hydroclimate variability in western North America during the Last Millennium, *J. Clim.*, *26*, 5863–5878, doi:10.1175/JCLI-D-11-00732.1.

Ault, T. R., J. E. Cole, J. T. Overpeck, G. T. Pederson, and D. M. Meko (2014), Assessing the risk of persistent drought using climate model simulations and paleoclimate data, *J. Clim.*, doi:10.1175/JCLI-D-11-00732.1, in press.

Becker, A., P. Finger, A. Meyer-Christoffer, B. Rudolf, K. Schamm, U. Schneider, and M. Ziese (2013), A description of the global land-surface precipitation data products of the Global Precipitation Climatology Centre with sample applications including centennial (trend) analysis from 1901-present, *Earth Syst. Sci. Data*, *5*, 71–99.

Bothe, O., J. H. Jungclaus, and D. Zanchettin (2013), Consistency of the multi-model CMIP5/PMIP3-past1000 ensemble, *Clim. Past Discuss.*, *9*, 2471–2487, doi:10.5194/cp-9-2471-2013.

Bunde, A., U. Büntgen, J. Ludescher, J. Luterbacher, and H. von Storch (2013), Is there memory in precipitation?, *Nat. Clim. Change*, *3*, 174–175, doi:10.1038/nclimate1830.

Castro, C. L., T. B. McKee, and R. A. Pielke Sr. (2001), The relationship of the North American monsoon to tropical and north Pacific sea surface temperatures as revealed by observational analyses, *J. Clim.*, *14*, 4449–4473, doi:10.1175/1520-0442(2001)014<4449:TROTNA>2.0.CO;2.

Coats, S., J. E. Smerdon, R. Seager, B. I. Cook, and J. F. González-Rouco (2013a), Megadroughts in southwest North America in millennium-length ECHO-G simulations and their comparison to proxy drought reconstructions, *J. Clim.*, doi:10.1175/JCLI-D-12-00603.1.

Coats, S., J. E. Smerdon, B. I. Cook, and R. Seager (2013b), Stationarity of the tropical Pacific teleconnection to North America in CMIP5/PMIP3 model simulations, *Geophys. Res. Lett.*, *40*, 4927–4932, doi:10.1002/grl.50938.

Coats, S., J. E. Smerdon, B. I. Cook, and R. Seager (2015a), Are simulated megadroughts in the North American Southwest forced?, *J. Clim.*, *28*, 124–142, doi:10.1175/JCLI-D-14-00071.1.

Coats, S., B. I. Cook, J. E. Smerdon, and R. Seager (2015b), North American pan-continental drought in model simulations of the Last Millennium, *J. Clim.*, *28*, 2025–2043, doi:10.1175/JCLI-D-14-00634.1.

Cook, B. I., and R. Seager (2013), The response of the North American monsoon to increased greenhouse gas forcing, *J. Geophys. Res. Atmos.*, *118*, 1690–1699, doi:10.1002/jgrd.50111.

Cook, B. I., R. Seager, R. L. Miller, and J. A. Mason (2013), Intensification of North American megadroughts through surface and dust aerosol forcing, *J. Clim.*, *26*, 4414–4430, doi:10.1175/JCLI-D-12-00022.1.

Cook, E. R., R. Seager, M. A. Cane, and D. W. Stahle (2007), North American drought: Reconstructions, causes, and consequences, *Earth Sci. Rev.*, *81*(1–2), 93–134.

Feng, S., et al. (2008), Atlantic and Pacific SST influences on Medieval drought in North America simulated by the Community Atmospheric Model, *J. Geophys. Res.*, *113*, D11101, doi:10.1029/2007JD009347.

Fernández-Donado, L., et al. (2012), Temperature response to external forcing in simulations and reconstructions of the Last Millennium, *Clim. Past Discuss.*, *8*, 4003–4073, doi:10.5194/cpd-8-4003-2012.

Foster, J., G. Liston, and R. Koster (1996), Snow cover and snow mass intercomparisons of general circulation models and remotely sensed datasets, *J. Clim.*, *9*, 409–426, doi:10.1175/1520-0442(1996)009%3C0409:SCASMI%3E2.0.CO;2.

Gochis, D., J. Schemm, W. Shi, L. Long, W. Higgins, and A. Douglas (2009), A forum for evaluating forecasts of the North American monsoon, *Eos Trans. AGU*, *90*(29), 249, doi:10.1029/2009EO290002.

Griffin, D., D. M. Meko, R. Touchan, S. W. Leavitt, and C. A. Woodhouse (2011), Latewood chronology development for summer-moisture reconstruction in the U.S. Southwest, *Tree-Ring Res.*, *67*, 87–101.

Griffin, D., C. A. Woodhouse, D. M. Meko, D. W. Stahle, H. L. Faulstich, C. Carrillo, R. Touchan, C. L. Castro, and S. W. Leavitt (2013), North American monsoon precipitation reconstructed from tree-ring latewood, *Geophys. Res. Lett.*, *40*, 954–958, doi:10.1002/grl.50184.

Gutzler, D. S. (2000), Covariability of spring snowpack and summer rainfall across the Southwest United States, *J. Clim.*, *13*, 4018–4027, doi:10.1175/1520-0442(2000)013<4018:COSSAS>2.0.CO;2.

Herweijer, C., R. Seager, E. R. Cook, and J. Emile-Geay (2007), North American droughts of the Last Millennium from a gridded network of tree-ring data, *J. Clim.*, *20*, 1353–1376, doi:10.1175/JCLI4042.1.

Higgins, R. W., and W. Shi (2000), Dominant factors responsible for interannual variability of the summer monsoon in the southwestern United States, *J. Clim.*, *13*, 759–776.

Kalnay, E., et al. (1996), The NCEP/NCAR 40-year reanalysis project, *Bull. Am. Meteorol. Soc.*, *77*(3), 437–471.

Kaplan, A., M. A. Cane, Y. Kushnir, A. C. Clement, M. Benno Blumenthal, and B. Rajagopalan (1998), Analyses of global sea surface temperature 1856–1991, *J. Geophys. Res.*, *103*(18), 18,567–18,589.

Kushnir, Y., R. Seager, M. Ting, N. Naik, and J. Nakamura (2010), Mechanisms of tropical Atlantic SST influence on North American precipitation variability, *J. Clim.*, *23*, 5610–5628.

Langford, S., S. Stevenson, and D. Noone (2014), Analysis of low-frequency precipitation variability in CMIP5 historical simulations for southwestern North America, *J. Clim.*, *27*, 2735–2756, doi:10.1175/JCLI-D-13-00317.1.

McKee T. B., N. J. Doesken, J. Kleist (1993), The relationship of drought frequency and duration to time scales, in *Proceedings of the Eighth Conference on Applied Climatology*, 179–184, Am. Meteorol. Soc., Boston.

Notaro, M., and A. Zarrin (2011), Sensitivity of the North American monsoon to antecedent Rocky Mountain snowpack, *Geophys. Res. Lett.*, *38*, L17403, doi:10.1029/2011GL048803.

Oglesby, R., S. Feng, Q. Hu, and C. Rowe (2012), The role of the Atlantic multidecadal oscillation on medieval drought in North America: Synthesizing results from proxy data and climate models, *Global Planet. Change*, *84–85*, 56–65.

Phipps, S. J., H. V. McGregor, J. Gergis, A. J. E. Gallant, R. Neukom, S. Stevenson, D. Ackerley, J. R. Brown, M. J. Fischer, and T. D. van Ommen (2013), Paleoclimate data–model comparison and the role of climate forcings over the past 1500 years, *J. Clim.*, *26*, 6915–6936, doi:10.1175/JCLI-D-12-00108.1.

Rasmusson, E. M., and T. H. Carpenter (1982), Variations in tropical sea surface temperature and surface wind fields associated with the Southern Oscillation/El Niño, *Mon. Weather Rev.*, *110*, 354–384, doi:10.1175/1520-0493(1982)110<0354:VITSST>2.0.CO;2.

Rudolf, B., H. Hauschild, W. Rueth, and U. Schneider (1994), Terrestrial precipitation analysis: Operational method and required density of point measurements, in *Global Precipitations and Climate Change*, *NATO ASI Series I*, vol. 26, edited by M. Desbois and F. Desalmond, pp. 173–186, Springer, New York.

Santer, B. D., K. E. Taylor, T. M. L. Wigley, J. E. Penner, P. D. Jones, and U. Cubasch (1995), Towards the detection and attribution of an anthropogenic effect on climate, *Clim. Dyn.*, *12*, 77–100.

Schmidt, G. A., et al. (2011), Climate forcing reconstructions for use in PMIP simulations of the Last Millennium (v1.0), *Geosci. Model Dev.*, *4*, 33–45, doi:10.5194/gmd-4-33-2011.

Schmidt, G. A., et al. (2013), Using paleo-climate comparisons to constrain future projections in CMIP5, *Clim. Past Discuss.*, *9*, 775–835, doi:10.5194/cpd-9-775-2013.

Seager, R., M. Ting, M. Davis, M. Cane, N. Naik, J. Nakamura, C. Li, E. Cook, and D. W. Stahle (2009), Mexican drought: An observational modeling and tree ring study of variability and climate change. *Atmósfera* [online], 22: 1, 1–31.

Sen Gupta, A., N. C. Jourdain, J. N. Brown, and D. Monselesan (2013), Climate drift in the CMIP5 models, *J. Clim.*, *26*, 8597–8615.

Stahle, D. W., M. K. Cleaveland, H. D. Grissino-Mayer, R. D. Griffin, F. K. Fye, M. D. Therrell, D. J. Burnette, D. M. Meko, and J. Villanueva Diaz (2009), Cool- and warm-season precipitation reconstructions over Western New Mexico, *J. Clim.*, *22*, 3729–3750, doi:10.1175/2008JCLI2752.1.

Stine, S. (1994), Extreme and persistent drought in California and Patagonia during medieval time, *Nature*, *369*, 546–549.

Sueyoshi, T., et al. (2013), Set-up of the PMIP3 paleoclimate experiments conducted using an Earth system model, MIROC-ESM, *Geosci. Model Dev.*, *6*(3), 819–836.

Taylor, K. E., R. J. Stouffer, and G. A. Meehl (2012), An overview of CMIP5 and the experiment design, *Bull. Am. Meteorol. Soc.*, *93*, 485–498.

Zhu, C., D. P. Lettenmaier, and T. Cavazos (2005), Role of antecedent land surface conditions on North American monsoon rainfall variability, *J. Clim.*, *18*, 3104–3121, doi:10.1175/JCLI3387.1.